Journal of Electroanalytical Chemistry 773 (2016) 69–78

Contents lists available at ScienceDirect

Journal of Electroanalytical Chemistry

journal homepage: www.elsevier.com/locate/jelechem

Oxygen evolution activity and stability of iridium in acidic media. Part 1. – Metallic iridium

Serhiy Cherevko [a,b], Simon Geiger [a], Olga Kasian [a,c], Andrea Mingers [a], Karl J.J. Mayrhofer [a,b,d]

[a] Department of Interface Chemistry and Surface Engineering, Max-Planck-Institut für Eisenforschung GmbH, Max-Planck-Straße 1, 40237 Düsseldorf, Germany
[b] Forschungszentrum Jülich GmbH, Helmholtz Institute Erlangen-Nürnberg for Renewable Energy (IEK-11), Egerlandstraße 3, 91058 Erlangen, Germany
[c] Ukrainian State University of Chemical Technology, Gagarin ave. 8, 49005 Dnipropetrovsk, Ukraine
[d] Department of Chemical and Biological Engineering, Friedrich-Alexander-Universität Erlangen-Nürnberg, Egerlandstr. 3, 91058 Erlangen, Germany

ARTICLE INFO

Article history:
Received 11 February 2016
Received in revised form 1 April 2016
Accepted 18 April 2016
Available online 19 April 2016

Keywords:
Iridium dissolution
Corrosion
Degradation
Oxidation
Oxygen evolution

ABSTRACT

A better understanding of iridium dissolution is important in the elucidation of the general mechanism of noble metals corrosion and in the design of more durable iridium based applied materials. In the current work iridium dissolution has been addressed by a complementary electrochemical and mass spectrometric technique based on a scanning flow cell (SFC) and inductively coupled plasma mass spectrometry (ICP-MS). Time- and potential-resolved iridium dissolution profiles are recorded and analyzed. It is found that during the anodic treatment dissolution is increasing constantly with potential. Anodic dissolution decreases with time, which is attributed to the buildup of a passivating oxide layer. In case a significantly low reductive potential is applied to the oxidized electrode, an additional dissolution process is observed. It is concluded that like other members of the noble metals group, e.g. gold and platinum, thoroughly studied before, dissolution of iridium is initiated by a change in the iridium oxidation state during the initial formation or reduction of a *thin compact anhydrous oxide layer*. Both transitions metal/oxide and oxide/metal during oxidation and reduction, respectively, result in dissolution. Thus, dissolution is a transient process. The Ir(III)/Ir(IV) transition in the *thick hydrous oxide layer*, responsible for iridium oxide electrochromism, do not lead, however, to any significant change in dissolution signal. At even higher anodic potentials, further destabilization is caused by a change in the oxidation number (increase and decrease) of iridium cations during oxygen evolution reaction (OER). At studied potentials OER on the metallic electrodes, covered by a *thin compact anhydrous oxide layer*, has Tafel slope of ca. 66 mV dec^{-1}, which is comparable to literature data on bulk IrO_2 electrodes and, probably, implies on similarities in the OER mechanism on these materials.

1. Introduction

Like other members of the platinum metals group, iridium is considered to be very noble. Indeed, this metal is even sometimes called to be "the most resistant of all metals to corrosion" [1,2], e.g. it does not dissolve in the *aqua regia* even at elevated temperatures [3,4]. According to the Pourbaix diagram, iridium is stable towards dissolution at pH = 0 in aqueous solutions, which do not contain complexing agents, up to potential of E° = 0.926 V [3]. Thermodynamically, the most stable phase of iridium up to E° = 0.926 V, at which oxidation to Ir_2O_3 and/or IrO_2 oxides (the former is not stable in presence of oxygen [5]) should take place, is metallic iridium [3]. Despite these facts, even the relatively early reports on electrochemistry of iridium noted its oxidation at significantly lower potentials [6]. It has been shown that in an acidic electrolyte adsorption of oxygen (or hydroxyl) on iridium electrode starts at potentials as low as 0.4–0.5 V [7–12]. Depending on the timescale of experiment, already at 0.6–0.65 V a monolayer coverage of O/OH has been reported [7]. Although, at typically employed scanrates in the potentiodynamic tests a monolayer coverage is completed at higher potentials of 1.1–1.2 V [8]. According to literature, formation of a "surface bulk phase" oxide through the so-called "place-exchange" process in the potentiodynamic treatment initiates at iridium at ca. 1 V against reversible hydrogen electrode (RHE) [8,13,14]. In all these aspects, iridium behaves similarly to platinum or gold, typically considered as model systems in electrochemical studies.

In comparison to these model systems, however, literature on the initial stages of iridium oxidation is scarce and contradictory. It is known, that electrochemistry of iridium in alkaline and acidic electrolytes is quite different, which means that transfer of knowledge collected in studies on different electrolytes is difficult. Based on the untypical shift of the main iridium oxidation peak with pH, the so-called "super-Nernstian" behavior of iridium was proposed by Burke et al. [15,16]. This was, however, questioned by Juodkazyte et al. [9]. Instead, explaining the pH dependence of the peaks, these authors concluded formation of different main compounds (having different redox potentials) in acidic and alkaline electrolytes. Another suggestion made by these authors is

E-mail addresses: cherevko@mpie.de (S. Cherevko), mayrhofer@mpie.de (K.J.J. Mayrhofer).

http://dx.doi.org/10.1016/j.jelechem.2016.04.033
1572-6657/

contrary to the usually proposed underpotentially deposited OH^- ions, "bulk" Ir hydroxides form on iridium [9,10]. Standard potentials of "bulk" $Ir(OH)_3$ and $Ir(OH)_4$ formation were found to be ca. 0.8 and 0.9 V [10]. To assist in the resolving of the complex electrochemistry of iridium, ellipsometry, electron diffraction, electron microscopy, X-ray or ultraviolet photoemission spectroscopy (XPS and UPS), and probe beam deflection (photothermal deflection spectroscopy) have been traditionally employed [11,12,17–22]. More advanced *ambient* or in-situ X-ray spectroscopy and X-ray diffraction methods are typically used nowadays [23,24]. In most of these studies, however, behavior of the iridium oxide but not iridium metal, as a starting material, in the potential region of OER was addressed [25–31]. Oxidation and reduction of metallic iridium was only studied in a few works, e.g. by electrochemical quartz crystal microgravimetry (EQCM) [9] or UPS [11]. The outcome of these studies is that electrochemistry of Ir/Ir (hydro)-oxide(s) system is complex. It is, probably, much more complicated than that reflected in the Pourbaix diagram.

The question arises, if metallic iridium is indeed stable to corrosion as it is traditionally believed. While dissolution of iridium at potentials exceeding 1.65–1.8 V_{RHE} [32,33] and dependence on the structure of oxide is well studied [34–36], little to nothing is known about corrosion of this metal at lower potentials. Dissolution of iridium has been mentioned (but not confirmed) in some studies on the oxidation or reduction of iridium [9,10,37–40]. Besides these studies, as discussed above, it is typically reported that this metal is very stable [41,42]. Stability is usually assumed based on the thermodynamic properties of iridium up to ca. 1 V and/or on the some preliminary data on the stability of the electrochemical current or potential profiles over, usually, limited time intervals. This general belief is probably one of the reasons why literature on the stability of iridium dissolution is so deficient. The other reason is a consequence of iridium low abundance and high price, making its use in practical applications undesirable. Nevertheless, potential utilization of iridium in electrocatalysis or photo-(electro)catalysis of OER is a heavily discussed topic nowadays [42–44]. As in these applications iridium exists in the form of oxide, its stability is out of the discussion of this part of the work (see Part II). In some other cases, however, metallic iridium is used. The use of small amounts of metallic iridium (usually in form of finely divided particles, other nanostructures, or in form of alloys) can be justified in view of its high activity, tolerance to methanol, reported stability, or other properties [45–53].

According to radio-chemical methods extensively used by Kolotyrkin and Chemodanov et al., iridium dissolution in acidic electrolytes containing no oxidizing agents initiates at ca. 0.6 V_{RHE} and accelerates with potential [12]. In line with their previous works on dissolution of platinum, gold, rhodium, and palladium [54,55], Rand and Woods reported that also iridium dissolves when the potential is cycled between 0.06 and 1.54 V_{RHE} [56]. Even though the authors suggested an existence of anodic or cathodic mode of dissolution, it was impossible to identify the dissolution process more precisely using the available technique. No time or potential resolved results were presented. The authors even wrote that "ring-disc studies would be required to identify positively the processes involved" [56]. Surprisingly, it took 40 years until such work has been partially completed. In a very recent paper, Danilovic et al. presented rotating ring-disk electrode (RRDE) results on iridium dissolution [27]. Unfortunately, only data on dissolution from electrochemically and thermally formed oxides in the region of OER was shown. Thus, no information related to the main topic of the current work, on the stability of metal itself was provided. In our previous work in which we summarized the results on the stability of a group of noble metals in the region of oxide formation/reduction and during the OER, we already presented that iridium behaves very similarly to platinum in the sense that predominant dissolution takes place in the cathodic branch of CV [55]. It was also reported that metallic iridium in the potential region of OER is less stable than chemically prepared iridium oxides [57,58].

In the current work we aim to extend the previously reported scarce studies showing dissolution of metallic iridium during initial stages of the surface oxidation and reduction of the formed oxide. Electrochemical growth of bulk hydrous oxide and iridium dissolution during the growth as well as during application of the oxide towards OER are presented in Part II.

2. Experimental details

All experiments were conducted using a scanning flow cell (SFC) inductively coupled plasma mass spectrometer (ICP-MS) based setup [59]. The SFC with V-shaped inlet-outlet channels was made in-house out of a polycarbonate block using a CNC-milling machine (CAM 4-02 Impression Gold, vhf camfacture AG, Germany). The small opening at the intersection of the channels, which defines the area of the working electrode, was ca. 0.01 cm^2. All data are normalized to this exposed geometric area of the working electrode. A commercial saturated Ag/AgCl electrode (Metrohm, Germany) and a graphitic rod were used as reference and counter electrodes, respectively. All potentials in this work are presented with respect to the reversible hydrogen electrode (RHE) potential, which was acquired against the Ag/AgCl electrode using a Pt disk working electrode (5 mm diameter disk sealed in Teflon®, MaTeck, Germany) after hydrogen saturation. During investigation of iridium dissolution, the electrolyte was pumped to/from the cell by a standard ICP-MS (NexION 300×, Perkin Elmer) pump with a constant flow rate of ca. 200 μL min^{-1} through Tygon® tubes (380 μm inner diameter) from a reservoir of argon-saturated electrolyte to the V-shaped channels of the polycarbonate cell and further downstream to the ICP-MS. The 0.1 M H_2SO_4 electrolyte was always freshly made by dilution of Suprapur® concentrated sulfuric acid (Merck, Germany) in ultrapure water (PureLab Plus system, Elga, 18 MΩ, TOC < 3 ppb). The on-line detection of concentration of dissolved iridium from the working electrode was performed by an ICP-MS, which was calibrated on each experiment day. 10 mg L^{-1} ^{187}Re was used as an internal standard (mixing ratio 1: 1). The lag time between SFC and ICP-MS was ca. 15 s and was always taken into account during construction of the potential/dissolution vs. time graphs presented in the paper. The potentiostat (Gamry Reference 600, USA), electrolyte, gas flow, and SFC positioning were automatically controlled using an in-house built LabVIEW software [60]. The working electrode was an iridium disk of 5 mm in diameter (MaTeck, Germany) embedded in a Teflon® cylinder for ease of handling. Before each experiment, the electrode was successively polished with 1 and 0.3 μm alumina suspensions on a polishing cloth (Struers, MD Mol) followed by a short sonication in water, extensive washing in the ultrapure water and drying in a flow of argon. Shortly afterwards the electrode was placed on an *xyz*-positioning table and a tungsten needle was connected to the conducting working electrode holder to make an electrical contact. No additional electrochemical pretreatment was done. More details on the cell design, the setup, and on the ICP-MS measurements can be found in the experimental parts of the previous reports [61–63].

3. Results

3.1. Oxidation and reduction of iridium studied by cyclic voltammetry

In our previous reports on the dissolution of gold and platinum we have shown that dissolution of these metals correlates well with oxidative and reductive processes taking place at the electrodes when potential is changed, e.g. in a simple cyclic voltammogram (CV) [61,62,64–68]. Therefore we start the study on iridium dissolution with investigation of iridium oxidation and reduction processes using the same technique. Typical CVs of a freshly polished polycrystalline iridium electrode acquired at a scan rate of $\upsilon = 50$ mV s^{-1} recorded right after 100 cycles at $\upsilon = 500$ mV s^{-1} up to upper potential limits (UPL) $1.1 \le E_{UPL} \le 1.6$ V_{RHE} with the constant lower potential limit (LPL) of $E_{LPL} = 0.04$ V_{RHE} are presented in Fig. 1 (results on the dissolution of iridium during the fast potential cycling to different UPLs are presented

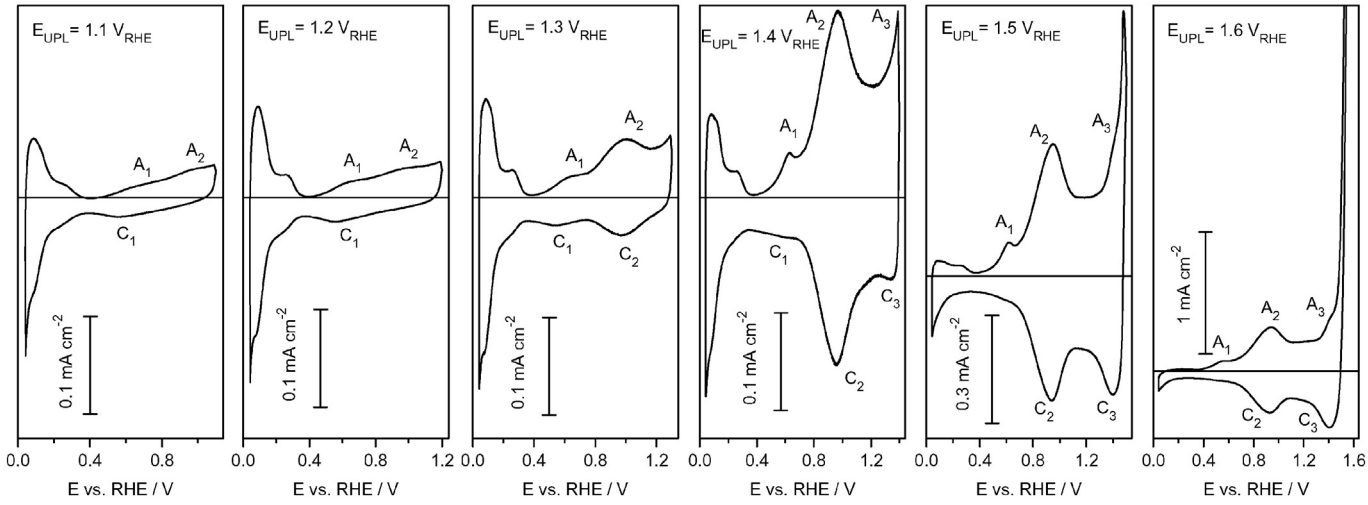

Fig. 1. Cyclic voltammograms showing the effect of upper potential limit of potential cycling on the voltammetry profile of iridium in 0.1 M H_2SO_4 electrolyte. Scan rate: 50 mV s^{-1}. Prior to taking the voltammograms potential was cycled 100 times in the same potential window at a scan rate of 500 mV s^{-1}.

in Fig. 3 in Part II). Metallic iridium, similarly to platinum and rhodium, is known to adsorb hydrogen in the so-called hydrogen underpotential deposition (H) region [69]. One can clearly see that the charge related to the adsorption/desorption of hydrogen increases with UPL up to E_{UPL} = 1.3–1.4 V_{RHE} and decreases afterwards when the UPL moves to the higher values. The initial increase may be related to surface cleaning, re-constructing, and/or roughening. The decrease of H_{UPD} charge with further increase in potential must be attributed to the blockage of the metallic surface sites situated underneath of the thick hydrous oxide layer (see Part II), as was pointed out by other researchers [17,20,56,70].

As it is well known in the electrochemistry of platinum, one can use H_{UPD} charge for a rough estimation of the so-called electrochemical surface area (ECSA) and, thus, roughness factor (R_f) of the electrode, that is, the ratio between the ECSA and the geometric surface area. For the normalization a charge of $Q(H_{UPD}) = 220\ \mu C\ cm^{-2}$ for a monolayer coverage of H on Pt is assumed. Similar procedure can be applied to estimate R_f of an iridium electrode. The important difference between these two metals is that in the fast potentiodynamic experiments the maximal coverage of hydrogen on iridium before the onset of hydrogen evolution reaction is assumed to be 0.65 [13,56,69]. Thus, R_f can be calculated as $Q(H_{UPD})/(220\ \mu C\ cm^{-2} \times 0.65)$, where $Q(H_{UPD})$ is in $\mu C\ cm^{-2}$. Although, taking into account that in some cases (as shown below), the apparent R_f is lower than one, in this case we suggest to use an alternative term, namely "relative population of iridium metallic cites available to H adsorption", P_H, defined the same as R_f. It is reasonable to assume that dissolution of iridium depends on the P_H (R_f) of the electrode (in the first approximation scales linear). Taking into account that all results in this work are presented normalized to the geometric surface area, we found it needful adding information on the R_f of iridium electrode after treatments shown in Fig. 1 (see Table 1).

It should be noted that the numbers presented in Table 1 are approximate values presented for a rough estimation of the electrode surface condition and iridium dissolution normalized to the ECSA, i.e. to get an intensive value of dissolution signal. Errors in ECSA (if any) may originate from differences in exact conditions used for its estimation. In the original work of Woods a slightly lower LPL and lower scan rates were used to obtain the maximal coverage of 0.65 [69]. Nevertheless, R_f values of 1.3 and 1.8 obtained for E_{UPL} = 1.1 and 1.2 V_{RHE} are close to that usually obtained on platinum [62,65,71,72]. These are probably the potential limits which should be used for cleaning of polished iridium electrode. One has to be aware, however, about the dissolution of iridium during such cleaning procedure (see Fig. 3 in part II) and its consequence on electrolyte purity. If the potential is cycled up to $E_{UPL} < 1.1$ apparent R_f is less than one, which suggests that hydrogen adsorption on the pretreated electrode is hindered. The total amount of adsorbed hydrogen on the electrode decreases when potential moves to even higher anodic values.

Unlike for platinum, the so-called double layer region of iridium is poorly defined. Going to higher potentials, an increase in the anodic current at E = 0.4 V_{RHE} may be assigned to the onset of OH/O adsorption or formation of iridium oxide/hydroxide on the electrode. These processes give rise to the two ill-defined anodic waves A_1 and A_2 with peaks at $E \approx 0.65$ and 0.95 V_{RHE}, respectively. In case the E_{UPL} does not exceed 1.2 V_{RHE}, only one broad cathodic peak C_1 at $E \approx 0.55$–0.57 V_{RHE} (with higher values for cycles with lower UPLs) can be identified on the negatively going branch of CVs. When higher UPLs are used, a clearly defined peak C_2 appears on the voltammograms. An additional pair of peaks A_3/C_3 emerges at potentials just slightly lower of the onset of oxygen evolution at $E \approx 1.45$ V_{RHE}. Similarly to the charge in the H_{UPD} region, charges related to all anodic and cathodic processes due to OH/O adsorption or desorption and surface oxidation or reduction are strongly dependent on the UPL of applied cycles. Most obvious is the increase in A_2/C_2 peaks, which is discussed more in detail in Part II.

Table 1
Approximate values of the charge obtained by integration of the hydrogen desorption profile and of the calculated "relative population of iridium metallic cites available to H adsorption", P_H, of the iridium electrode after 100 cycles up to a potential indicated in the topmost raw of the table.

E vs. RHE/V	0.5	0.7	0.9	1.0	1.1	1.2	1.3	1.4	1.5	1.6
$Q(H_{UPD})/\mu C\ cm^{-2}$	14	13	13	36	180	250	290	260	170	>80
P_H (R_f)	0.1	0.1	0.1	0.25	1.3	1.8	2.0	1.8	1.2	>0.6

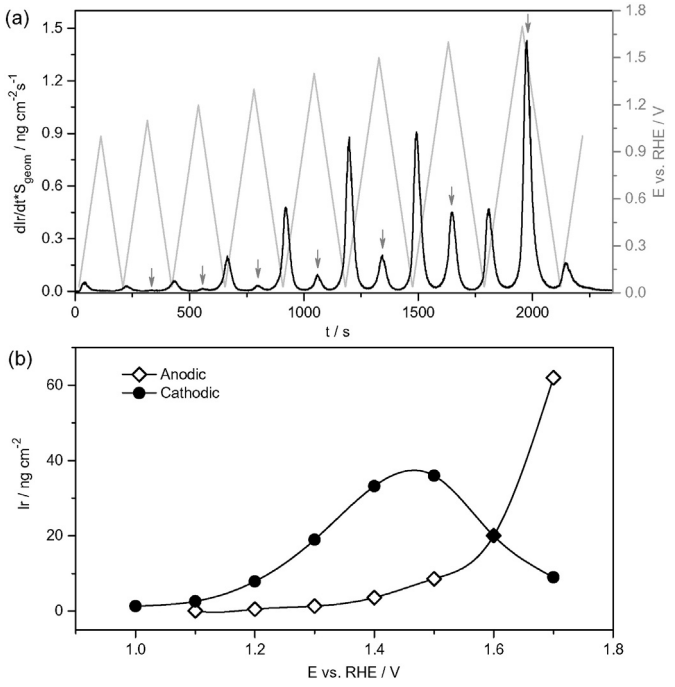

Fig. 2. Effect of the upper limit of potential cycling on dissolution of iridium. Iridium dissolution profile and applied potential program are shown in black and grey in (a), respectively. Arrows in (a) indicate peaks corresponding to the anodic range of potential. (b) Dependence of amount of iridium dissolved in the anodic and cathodic parts of cyclic voltammograms on upper potential limit of potential cycling. Amounts are obtained by integration of corresponding peaks presented in (a). Scan rate: 10 mV s^{-1}.

3.2. Dependence of iridium dissolution on potential during potentiodynamic conditions

In order to get a first insight on the electrochemical dissolution of iridium and its dependence on potential, a simple experiment consisting of successive CVs with each subsequent cycle having 0.1 V higher UPL than the preceding one was undertaken (Fig. 2).

The applied potential program with $1.0 \le E_{UPL} \le 1.7$ V_{RHE} is marked in grey in Fig. 2a. The iridium dissolution profile is presented in black in the same graph. The peaks originating from iridium dissolution at anodic potentials are marked by arrows. One can see that the initial potential excursion does not lead to any significant increment of iridium concentration in electrolyte. On the other hand, there are clearly visible peaks in the cathodic region of potential, both, in the beginning of the first cycle and in the end. This behavior of iridium can be explained assuming that there is presence of a native iridium oxide formed in air in time between polishing and measurement. Electrochemical dissolution of this oxide or chemical or electrochemical dissolution of another transient oxide formed on the way of the iridium oxide reduction to its metallic state is probably the main cause of the observed increase in dissolution signal. Assuming that not all oxide is reduced at the beginning of the first cycle, a new excursion in the cathodic region of potential should result in additional dissolution. Indeed, this is what happens at the end of the first cycle. As a confirmation of this assumption one can compare peaks originating from native oxide dissolution in different experiments (see for instances Fig. 3 and Fig. 5). The amount of cathodically dissolved iridium is higher when the experiment starts with a cathodic step aiming to reduce iridium oxide. In the range of $1.1 \le E_{UPL} \le 1.4$ both the anodic and cathodic peaks increase with potential. Thus, $E = 1.1$ V_{RHE} may be assigned as the onset potential of anodic iridium dissolution in potentiodynamic experiments. While anodic peak growth accelerates, the cathodic peak diminishes with further increase in the UPL. This is clearly seen after the integration of the corresponding peaks which provides information on the amount of dissolved material in the anodic and cathodic branches of a single cycle. Corresponding data is shown in Fig. 2b.

3.3. Resolving dissolution in anodic and cathodic potential regions

To clearly separate the peaks originating from dissolution of the native oxide and from oxidation of metal as well as the reduction of the formed oxides, a slightly different potential program was used. The potential was held at a cathodic potential for 300 s to ensure full reduction of the native oxide, followed by two cycles at a low scan rate of 2 mV s^{-1}. The corresponding program and dissolution signal are shown in grey and black in Fig. 3, respectively. In line with the results shown in Fig. 2, as soon as the contact between electrode and electrolyte is established, some iridium appears in electrolyte, resulting in a peak in the mass-spectrogram. Amount of dissolved material in this peak is ca. 6.9 ng cm^{-2}. Taking the weight of one monolayer of Ir of ca. 400 ng cm^{-2} (assumed using reported data on surface density of platinum atoms and taking into account similarities between iridium and platinum lattice parameters) one gets that only 1–2% of monolayer is dissolved. Amount of oxygen originally present on iridium must be significantly higher [73]. It may be suggested that after a short time in air the predominant part of oxygen is in the adsorbed states, which does not lead to a significant surface destabilization and dissolution during iridium reduction. At the same time, re-deposition of dissolved iridium, resulting in a decrease of its amount in electrolyte, cannot be ruled out. Similarly to the results shown in Fig. 2, in potentiodynamic experiments cathodic dissolution is the main cause of iridium loss at lower UPLs. At the scan rate of 2 mV s^{-1} and $E_{UPL} = 1.2$ V_{RHE}, amount of anodically dissolved iridium is an order of magnitude lower than that during the reduction of oxide. The difference decreases to just a factor of 2 at $E_{UPL} = 1.6$ V_{RHE}, even though both peaks are higher in this case. There are several interesting observations to be noted. As can be clearly seen from the graph, cathodic dissolution starts at a very low potential during the reductive branch of the CV. This finding is in line with known information on reduction of iridium oxide, which is kinetically hindered even at very low cathodic potentials [58]. This explains the very long signal tailing in the end of the experiment, confirming the early suggested hypothesis on the transient nature of noble metals dissolution taking place only during transition in oxidation state [55]. Kinetic hindrances of oxide reduction slow down dissolution. Another interesting finding is that the form of the anodic and cathodic peaks is substantially different. While the cathodic peak shows an exponential increase with potential going down to more cathodic values, there are several regions of different slopes in the anodic peak region. A slow increase in the dissolution signal with potential is observed already at ca. 0.7–0.8 V_{RHE}, with an acceleration of anodic dissolution at ca. 1.3 and 1.5 V_{RHE}. In general, this is in line with results presented in Fig. 2b. The onset of cathodic dissolution is around $E = 0.7$–0.8 V_{RHE}, the exact value depends on the electrode prehistory. It seems like it shifts to lower potentials for higher UPLs.

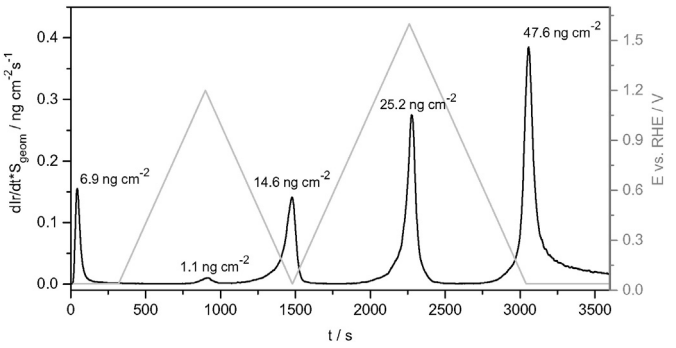

Fig. 3. Iridium dissolution (black line) during slow potential scan of 2 mV s^{-1} up to 1.2 and 1.6 V_{RHE} (applied potential program is shown in grey). Numbers present the amounts of dissolved iridium in each peak.

Comparing results presented in Figs. 2b and 3 one may notice some discrepancy in the amounts of dissolved material for the cycles with the same UPL. As an example, amount of cathodically dissolved iridium at $E_{UPL} = 1.6\ V_{RHE}$ in Fig. 3 is two times higher than that in Fig. 2b. There are two moments to be highlighted explaining these results. Firstly, two different scan rates were used. Secondly, pre-history for cycles with $E_{UPL} = 1.6\ V_{RHE}$ is different. Both of them may lead to different amount of accumulated iridium oxide not completely reduced in the preceding cycles. Additional reason to be mentioned is the difference in the dissolution onset potentials. This is also related to the scan rate dependent extent of surface oxidation [7].

3.4. Effect of scan rate of potential cycling on iridium dissolution rate

Fig. 4 shows the response of dissolution signal on the change of scan rate with which CVs were recorded. As only at lower scan rates it is possible to resolve between different processes, data for anodic and cathodic dissolution is presented for $\upsilon \leq 20\ mV\ s^{-1}$, while only summarized results are shown for the higher υ. In Figs. 2 and 3 we have shown that the main dissolution process is cathodic dissolution. It is not surprising, thus, that the profile showing the dependence of total amount of dissolved iridium on scan rate mimics that of cathodic dissolution. Both decrease significantly up to $\upsilon = 20\ mV\ s^{-1}$, and stabilize at higher scan rates. This suggests that dissolution takes place predominantly during the cathodic steps between the cycles. Anodic dissolution shows only little decrease with scan rate.

3.5. Dependence of iridium dissolution on potential during potentiostatic conditions

To clarify on the effect of residual oxide on dissolution of iridium, potentiodynamic experiments were complemented with potentiostatic ones, as shown in Fig. 5. Three different potential protocols were applied. Namely, (I) a stepwise increase in potential (Fig. 5a), (II) a stepwise increase in potential with steps separated with a step to a potential close to that of the open circuit potential (5b), and (III) experiment similar to the previous one, only that instead of the open circuit potential a significantly cathodic value was applied (Fig. 5c). Fig. 5a'–c' shows corresponding dependences of dissolved iridium against the potential of anodic step. Interestingly, while there is an obvious difference in the amounts of dissolved iridium in the anodic and cathodic steps, qualitatively, the dissolution picture remains the same, independent on the potential program applied. In all cases the onset of anodic and cathodic dissolution is at ca. 0.9 V_{RHE}. There is some dissolution at lower potentials, but amounts are negligibly small. Starting from 0.9 V_{RHE}, the anodic dissolution signal constantly grows and the dissolution rate accelerates at $E = 1.4–1.5\ V_{RHE}$. Similarly, there is an increase in cathodic dissolution but only till $E = 1.2\ V_{RHE}$. At higher UPLs the decrease in amount of dissolved material with potential can be clearly seen. In accordance with the previous results, cathodic dissolution is significantly higher when cathodic potential is lower. Comparing the last two programs, one can clearly see that in the case more oxide is reduced in the preceding cathodic pulse, anodic dissolution rate is higher in the following anodic step.

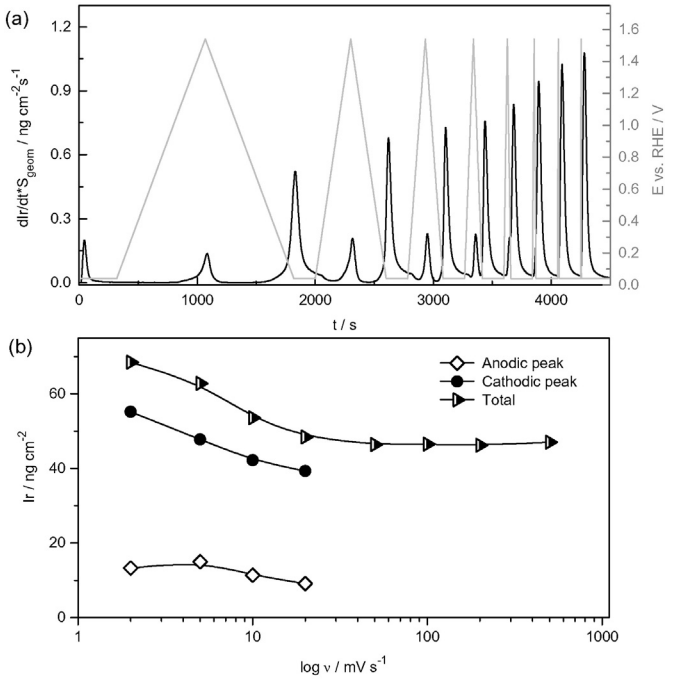

Fig. 4. Effect of potential scan rate on iridium dissolution. Iridium dissolution profile and applied potential program are shown in black and grey in (a), respectively. (b) Dependence of amount of iridium dissolved in the anodic and cathodic parts of cyclic voltammograms as well as total dissolved amount in one cycle on the potential scan rate. Amounts are obtained by integration of corresponding peaks presented in (a).

3.6. Activity and stability of iridium during oxygen evolution reaction

Electrocatalytic activity towards OER and stability of iridium is of high technological importance. Both of these parameters are tested here by applying prolonged anodic galvanostatic pulses. Fig. 6a shows dissolution of iridium at different applied currents. In the beginning of each experiment the surface of iridium was treated cathodically to remove the native oxide. During this step some dissolution was recorded, similar to that described above. In these measurements dissolution rate was found to cease to a value below detection limit of ICP-MS just in a few minutes, probably, indicating the complete reduction of iridium oxide [58]. With application of a galvanostatic step a sharp increase in dissolution was observed. In the first seconds, when surface is not covered by a compact protective oxide, direct electrochemical dissolution of iridium metal can be suggested as the major cause of the increment in the dissolution signal. Reversible potential of this reaction $E°(Ir/Ir^{3+}) = 1.156\ V_{SHE}$ [3]. The dissolution rate, however, decreases significantly with time, due to the development of a protective passive oxide layer on the electrode. Potential-time profiles presented in Fig. 6b–c confirm this assumption. Growth rate of oxide depends on applied current. At lower currents the major part of the current accounts for oxide formation. Thus, as shown in Fig. 6c, at $j = 0.1\ mA\ cm^{-2}$ potential is increasing gradually over the first 20 s until it reaches a value at which OER is the main reaction. On the other hand, at the highest currents of 0.5 and 1 $mA\ cm^{-2}$ it is virtually a couple of seconds till the signal is stabilized. Although, as can be seen in Fig. 6b, independent on current, some increase in potential is observed throughout the experiment, which indicates an increase in oxide thickness and/or change in its structure. This results in a constant decrease in the dissolution signal.

For all currents, after a first couple of minutes of experiment, the potential rises to ca. 1.5–1.6 V_{RHE}, which is in the region of increased iridium dissolution as discussed above. As was shown in Fig. 1, at potentials $E > 1.45\ V_{RHE}$ there is a significant increase in OER current, thus it can be concluded that it is oxygen evolution which is the main reaction in the experiments presented in Fig. 6 at all applied currents. By measuring the electrode potential at the end of each anodic pulse and plotting obtained values against logarithm of current one may estimate a Tafel slope for the OER. It should be noted that only one order of magnitude current is used in this case. As presented in Fig. 6c, $b = d(E)/d\ln(j) = 66\ mV\ dec^{-1}$ was obtained, which is similar to that reported in literature for bare iridium electrodes [36]. This value, however, should be taken with care as it depends on oxide thickness, which, as can be assumed from the i(t) profiles, is different at different currents. According to Damjanovic et al. [74,75] $E = 1.5–1.6\ V_{RHE}$ is exactly the region in which a transition of the Tafel slope from 40 to 120 $mV\ dec^{-1}$ occurs, indicating a change in the rate determining step of OER. Similar

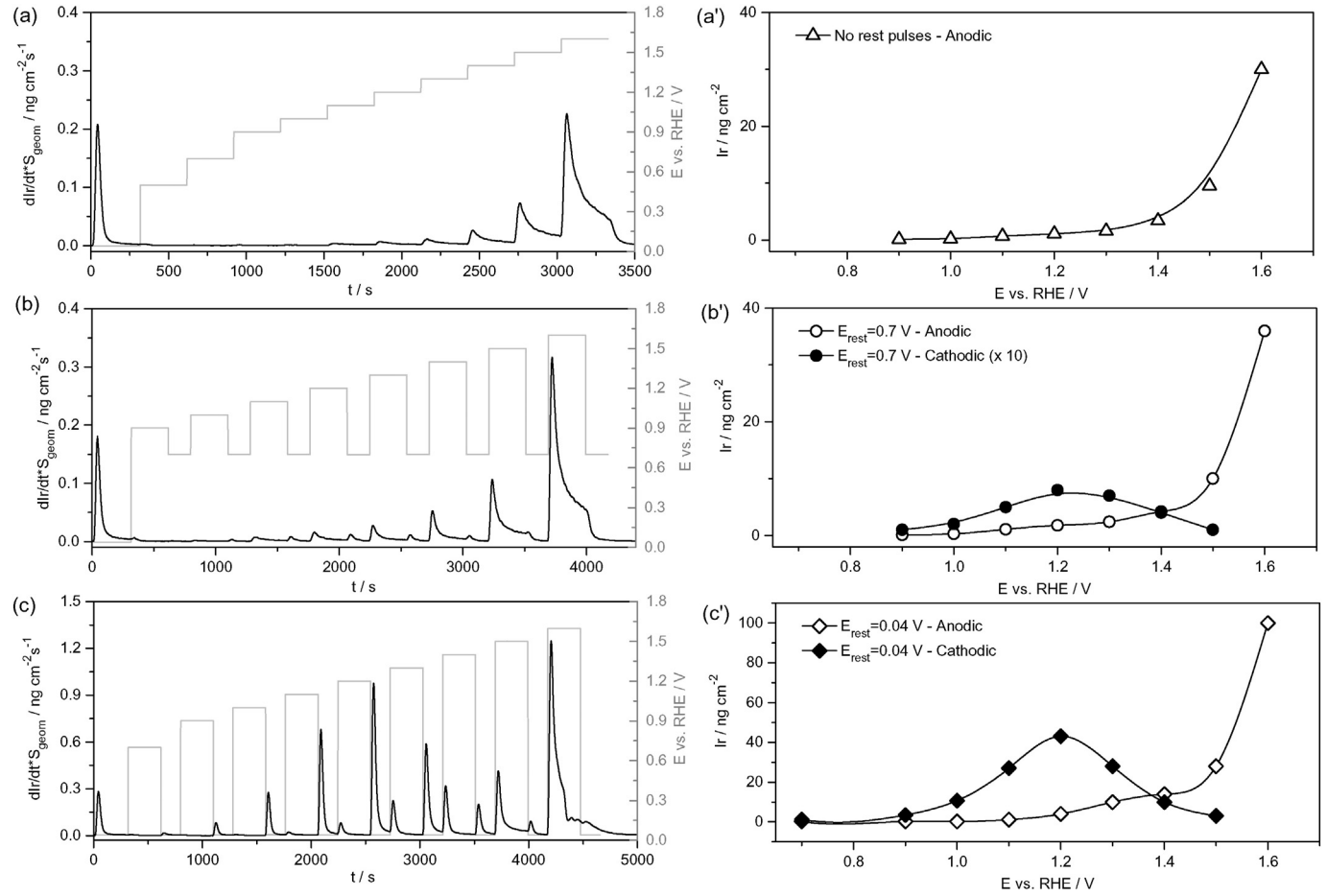

Fig. 5. Dependence of iridium dissolution on anodic and cathodic potential in different potential step experiments. (a) Stepwise increase in anodic potential. (b) Stepwise increase in anodic potential with cathodic potential holds at E = 0.7 V_{RHE} between each increase. (c) Same with (b) but cathodic hold potential is E = 0.04 V_{RHE}. In (a–c) iridium dissolution profile and applied potential program are shown in black and grey, respectively. (a'–c') Dependence of amount of iridium dissolved in anodic and cathodic steps on the value of anodic potential. Amounts are obtained by integration of corresponding dissolution profiles presented in (a'–c').

conclusion, even though the absolute values of the Tafel slopes were different, was made by Gottesfeld and Srinivasan [19].Taking into account that oxide formation rate accelerates at slightly lower potentials [74], this change in the mechanism may be due to the change of surface at which OER predominantly takes place [19]. In comparison to the hydrous iridium oxide electrode which, depending on thickness of oxide show Tafel slopes as low as 50 to 40 mV dec^{-1} (see Fig. 6 in Part II), metal electrode covered by a thin oxide layer show similar performance to that of chemically prepared IrO_2 OER catalyst [76].

4. Discussion

The most important information which should be discussed is:

(a) Potential at which transitions between different oxidation states and/or structure or composition take place and their effect on dissolution;

(b) The nature of formed adsorbed species and "bulk phase" oxides/hydroxides;

(c) Onset and mechanism of OER related to iridium dissolution.

4.1. Potential dependent iridium oxide formation/reduction and corresponding dissolution

4.1.1. Oxide formation region

Prior to going into details on iridium dissolution, it is advisable to focus on the oxidation/reduction of iridium and OER electrochemistry on the formed oxides, as these are the main processes directly affecting stability [55]. As we have shown for platinum and gold, there are usually some characteristic potentials pointing at the initiation of processes at which dissolution rate changes significantly [71]. Transition from the "adsorbed" to "bulk" oxygen state is one of such important processes. On noble metals such transformation is believed to happen through an interfacial place-exchange process [13,77–79], though, other mechanisms are also suggested (e.g. see Refs. [80–82] and references therein). Independent on the exact mechanism of the transition, it can be usually tracked using electrochemical methods [79,83]. It was suggested that unlike platinum and gold in acidic electrolytes, an appreciable amount of *reversibly adsorbed* OH/O can be detected on an iridium electrode in the potential range of 0.4 ≤ E ≤ 1.0 V_{RHE} or even higher [8,11,14]. According to literature, slow place-exchange (formation of "bulk phase") during potentiodynamic treatment starts at iridium at E ≥ 1 V_{RHE} [13]. All these values, however, should be taken with care, as place-exchange rate or oxygen coverage increase are kinetically hindered processes [7], especially at lower potentials, and, thus, its rate (also the assigned onset potential) depends on the timescale of experiment, e.g. scan rate of cycles. According to Conway et al., place-exchange is a stochastic process and the probability of an event to occur increases with time [84]. This is probably the main reason why the onset of iridium dissolution is different for potentiodynamic experiments conducted at different scan rates as shown in Figs. 2 and 3 and potentiostatic measurements presented in Fig. 5. The timescale for the latter one is significantly longer, so the amount of place-exchanged iridium sites is higher. This also explains why the onset of iridium dissolution measured by Chemodanov et al. [85] in the *prolonged* potentiostatic experiments is

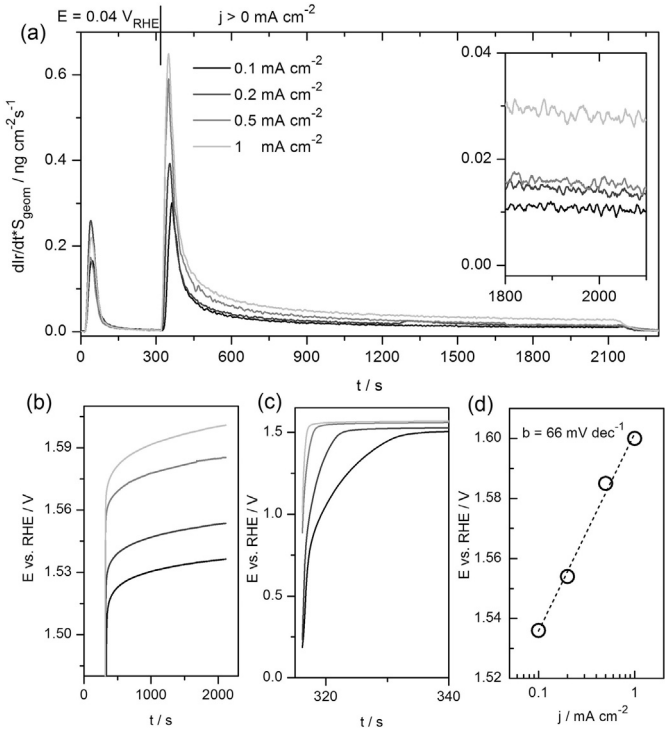

Fig. 6. (a) Dissolution of iridium during application of galvanic steps of $0.1 \le j \le 1$ mA cm^{-2}. Prior to each pulse the electrode potential was E = 0.04 V_{RHE}. (b) Change of the potential corresponding to the galvanostatic pulses. (c) Magnified view of (b) highlighting the potential variation during initial stages of oxide formation and dissolution on iridium. (d) Tafel plot obtained by presenting electrode potential measured at the end of each galvanostatic step against the applied current. The value of obtained Tafel slope is presented in (d).

0.6 V_{SHE} (in 0.5 M H_2SO_4), which is slightly lower to that found in the current work. Another difference between the measurements shown in Figs. 2 and 3 and Fig. 5 is the rate with which the highest potential is achieved. In the potentiostatic experiment the potential is changed at a very high rate to the value of interest, which may lead to non-equilibrated processes on the electrode causing dissolution or, oppositely, fast passivation. In potentiodynamic measurements, however, time scale of potential change is usually orders of magnitude lower. Independent of the potential mode, amount of bulk oxide is increasing with potential resulting in higher dissolution rates at higher potentials.

4.1.2. Oxide reduction region

The mechanism of cathodic iridium dissolution is probably similar to that suggested for other noble metals, like platinum and gold [61,62,65–68,71,86]. It should be noted, however, that even for these well studied materials the mechanism is not completely resolved. According to our recent hypothesis, transient dissolution is a process in which a short-lived instable metal oxide or hydroxide is chemically or electrochemically dissolved [71]. Reduction of iridium oxide is a kinetically hindered process. Even though thermodynamically iridium oxide is unstable at E° < 0.926 V [3], in reality it is very difficult to remove iridium oxide from the electrode even at much lower potentials [58]. Consequently, reduction usually takes place at potentials corresponding to the H_{UPD} potential region. In general, stability of an oxide depends on potential it was formed at. Usually, oxides formed at higher potentials reduce at lower cathodic potentials – a process similar to that observed in magnetization of a ferromagnetic. If we compare obtained values for the onset of cathodic dissolution (Fig. 3) with potentials of oxide reduction peaks C_1-C_3 (Fig. 1), we find that cathodic dissolution is initiated in/by the process taking place in peak C_1. It is most likely that this is the reduction of the compact iridium oxide similar to that formed on platinum (peak at ca. 0.75 V_{RHE} [71]). With increase in the UPL, C_1 peak position shifts to more negative values, at least for $E_{UPL} \le 1.3$ V_{RHE}, indicating the formation of a more stable oxide. Even though it is impossible to identify C_1 peak position for higher UPLs, it may be suggested that this trend extends also in this potential region. It is reasonable to suggest, assuming that electrodeposition of dissolved iridium species is controlled by electrochemical kinetics and not diffusion or some chemical processes in electrolyte, that the rate of re-deposition, or the ratio between deposited and dissolved ions, is higher at lower cathodic potentials. We also assume, for simplicity, that electrodeposition is a classical potential dependent process unlike, e.g. adsorbed hydrogen dependent deposition of iridium chloro complexes [40,87]. This information can be used to explain an observed bell-like shape of cathodic dissolution vs. potential dependence. With increase in UPL a more compact oxide is formed and reduced at the electrode. Consequently, the rate of cathodic dissolution grows with potential, e.g. like in the case of platinum dissolution in acidic solution [62]. It is usually assumed that a compact oxide on noble metals grows to some limited thickness. In particular a thickness of 3 monolayers, assuming oxide to be IrO_2, was reported [13]. In this case, saturation in cathodic dissolution should be observed, like for instance in case of platinum in alkaline electrolyte [71]. This shift of the oxide reduction peak to more negative values, however, may lead to higher ratios between re-deposited and dissolved species. This will result in lower detected amounts for higher UPLs. Finally, formation of porous hydrous oxide on top of a compact layer should lead to even higher ratios. We assume that dissolved species originate from dissolution of the compact oxide situated between metal and hydrous oxide. Thus, to be detected by ICP-MS, they have to be transferred to the bulk electrolyte. The presence of hydrous oxide may hinder mass-transfer. This should depend on the thickness of the oxide as discussed in part II. Moreover, re-deposition of dissolved species within the hydrous oxide may also be suggested. In case the electrode potential drops at the compact oxide/hydrous oxide interface rather than the hydrous oxide/electrolyte interface [88–90] (oxide is "turned off" [8,14,91]), however, such electrochemical re-deposition is, probably, negligible. As a confirmation of this suggestion, in part II we show that presence of thick hydrous oxide does not significantly influence the shape of cathodic dissolution profile. Besides re-deposition, an incomplete reduction of compact oxide formed at higher potentials may lead to a similar trend. If one assumes that the ratio between reduced and unreduced species decreases with UPL, amount of cathodically dissolved iridium should also decrease with UPL. This is due to generally observed correlation between the amount of oxide and cathodic dissolution [62]. As, according to Pickup and Birss [13], growth of hydrous oxide is initiated by incomplete reduction of compact oxide, such assumption seems to be plausible. In summary, most of the phenomenon discussed above can explain the observed bell-like shape of the cathodic dissolution profile.

Reductive processes in peak C_2 do not lead to any significant increase in cathodic dissolution. It may be suggested that oxides formed in this transition are quite stable or that transition is very fast. Reversibility of the peaks indeed confirms that electron/proton transfer is very fast in this process. Reduction of oxide in peak C_3 takes place at significantly high anodic potentials. In this case it is difficult to resolve dissolution events corresponding to anodic and cathodic processes. Anodic dissolution in this potential region accelerates with OER.

4.2. Nature of formed oxide species

So far we constructed our discussion without specifying compounds consumed/formed in the anodic and cathodic processes and responsible for the observed peaks on the voltammograms. In several last decades many reactions pathways and formation of different oxides, hydroxides, oxy-hydroxides, and hydrated oxy-species were suggested to explain iridium electrochemical profiles. In most of the cases pure electrochemical methods were complemented by surface science techniques to elucidate oxidation state of metals, content of oxygen or hydrogen and so on [11,20–22,25–31]. It is now generally accepted that adsorption of

O/OH starts at relatively low potential on iridium [11]. Hence, analyzing Fig. 1, peak A_1 may be ascribed to O/OH chemisorption. It is most likely that the amount of the "bulk phase" oxide formed through place-exchange is relatively low at this potential. Although, taking the stochastic nature of place-exchange into account, absence of such oxide cannot be ruled out, especially in long time intervals. Place-exchange accelerates at ca. 1 V_{RHE} [13]. It is assumed that the oxide formed as a result is anhydrated IrO_2 [88]. In case UPL of cycles is not higher than ca. 1.1 V_{RHE}, the formed oxide is reduced almost completely in the following cathodic ramp. At higher potentials, however, stable hydrous Ir(III) species form ($Ir(OH)_3$ and $HIrO_2$ are typically suggested, see part II for a more detailed discussion), which are not reduced in the cathodic branch of the CVs [13,21]. Facile protonation and deprotonation of this hydroxide, most likely with formation of $IrO(OH)_2$ or $IrO_2 \cdot H_2O$ [21], in acidic electrolyte is evidenced by reversible peaks A_2/C_2. Appearance of another pair of peaks A_3/C_3 at potentials preceding OER strongly suggests that this reaction takes place not on/from $IrO(OH)_2$ but on/from another oxide formed by oxidation of $IrO(OH)_2$, such as $IrO_2(OH)$ [21]. Usually, it is assumed that iridium cations have an oxidation state higher than four at these potentials [33], as an example, Ir(V) complexes were suggested [26,29,92]. Kötz et al. suggested the existence of Ir(VI) as in IrO_3 obtained by three deprotonation steps [21]. All these complexes are short-lived and decompose to molecular oxygen and an iridium complex with a lower oxidation state. As discussed in part II, formed intermediates may have lower stability and thus result in dissolution of iridium during OER. Discussed above is visualized in a simplified drawing shown in Scheme 1.

4.3. Oxygen evolution on metallic iridium covered with a thin oxide layer

According to Pickup and Birss, the growth mechanism of compact "bulk phase" inner oxide on iridium is similar to that on platinum [13]. Unlike platinum oxide, however, which completely reduces in the cathodic branch of voltammograms, iridium oxide formed at the higher potentials may reduce only partially. Partial conversion of compact oxide to a thin hydrous oxide in each consecutive cycle leads to formation of the thick porous hydrous oxide on top of a compact inner anhydrous oxide [13,93] (see also part II). It is assumed that such transition takes place at $E > 1.2$ V_{RHE} as a result of compact oxide's surface oxidation to a higher oxide with an almost immediate hydration. Moreover, it was reported that formation of such oxide coincides with the oxygen evolution at iridium [13]. If this is the case, some increase in iridium dissolution should be observed at these potentials, as the onset of oxygen evolution usually goes hand in hand with increased dissolution of noble metals [55]. As one can see from Fig. 1, formation of hydrous oxide is accelerated when $E_{UPL} \geq 1.4$ V_{RHE}. Data from both potentiostatic and potentiodynamic experiments are in good agreement, for both the slope of iridium dissolution curve becomes steeper at these potentials.

Regarding OER on the *uncycled* metallic electrodes, an increase of potential in positive direction should lead to growth of compact anhydrous thin oxide, similar to that formed on platinum. At higher potentials, it can be suggested that the oxygen evolution takes place on this oxide (at least partially [94]) but *not from* the oxide itself, as in the case of hydrated iridium oxide electrode (see Part II). The situation is rather similar to OER on "dry" IrO_2. The Tafel slope of OER in this case is usually relatively high. Increased dissolution of iridium during OER on compact oxide (in comparison to thermo-chemically formed IrO_2) may be due to metal cations migration/diffusion through the compact oxide under the electric field. Migration, however, can be questioned, assuming that the compact oxide is a good electronic conductor. Chemical dissolution of the compact IrO_2 is assumed to be low but it can be accelerated due to a possible local pH increase during OER. This increase may also accelerate proton dependent electrochemical dissolution of IrO_2 [3]. Taking into account, however, that there is no porous network at the surface of the electrode, local increase in pH in well buffered

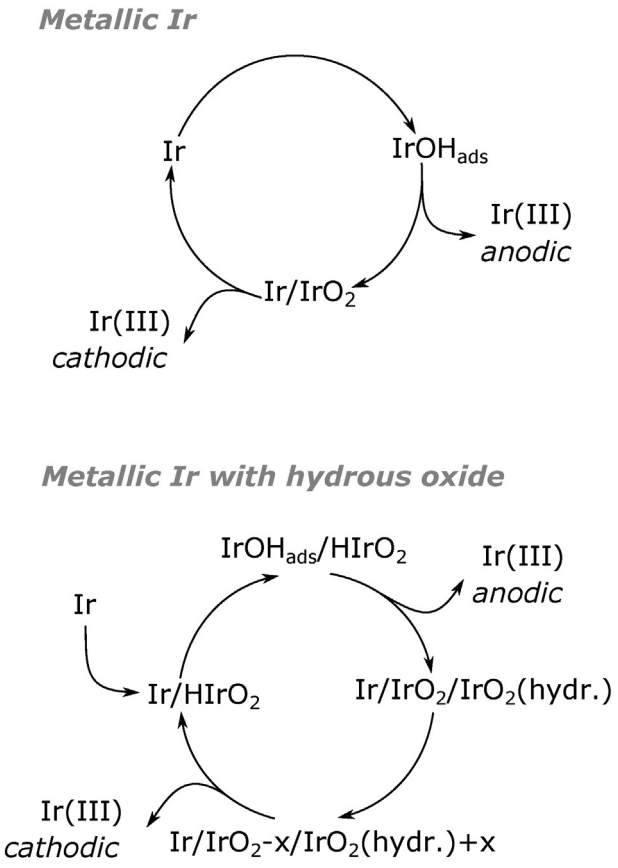

Scheme 1. A simplified sketch on the suggested dissolution processes during cycles without (top pane) and with (low pane) hydrous oxide buildup on an iridium metal electrode. Symbol "x" represents the fraction of "dry" IrO_2 converted to hydrated IrO_2(hydr.).

electrolyte is unlikely. With increase in OER some IrO_2 probably hydrates. Such effect is known in electrochemistry of Pt and Au, where formation of hydrous oxide is possible at a constant potential [95]. In this case the coexistence of two mechanisms of OER may be suggested. The amount of such hydrous oxide is however limited. It may explain transition in the OER mechanism reported in literature [75]. The change in ratio between the two processes is probably the main reason of Tafel plot variation with oxide thickness (see part II). A Tafel slope of ca. 118 mV dec^{-1} found at higher overpotential on oxidized iridium [75], suggests, that the formed hydrous oxide is most likely dissolved and that the main mechanism is formation of oxygen molecules *from water* on the surface of the oxide, not from the oxide itself [55].

5. Conclusions

The results of our investigation of polycrystalline iridium metal electrode by SFC-ICP-MS have shown that with increase in the electrode potential iridium dissolution initiates at potentials of ca. 0.7–1.1 V_{RHE}. The exact onset potential depends on the time scale of the experiment and is lower for longer anodic polarizations. Dissolution increases gradually with potential up to 1.4–1.5 V_{RHE}. The first onset of dissolution is attributed to advent of bulk oxide formation, most likely, through the interfacial place-exchange mechanism. The acceleration in the dissolution signal at more positive potentials is suggested to be related to the onset of oxygen evolution reaction. In both cases participation of an instable intermediate during the compact oxide formation and oxygen evolution is hypothesized. Reduction of oxide during the cathodic treatments results in a transition from the oxide to metallic iridium through formation of probably the same unstable complex and its partial dissolution. Observed bell-like shape of dissolution against potential is

explained by re-deposition of dissolved species and/or non-complete reduction of the oxide.

Acknowledgements

The authors acknowledge the BMBF (Kz: 033RC1101A) for financial support. K.M. acknowledges financial support from the DFG under the project number MA4819/4-1. O.K. acknowledges financial support from the Alexander von Humboldt Foundation. S.G. acknowledges financial support from the BASF.

References

[1] L.B. Hunt, A history of iridium, Platin. Met. Rev. 31 (1) (1987) 32–41.
[2] D.R. Lide, CRC Handbook of Chemistry and Physics, 85th ed. Taylor & Francis, 2004.
[3] M. Pourbaix, Atlas of Electrochemical Equilibria in Aqueous Solutions, National Association of Corrosion Engineers, 1974.
[4] S.B. Lyon, Corrosion of noble metals*, in: B. Stott, M. Cottis, R. Graham, S. Lindsay, T. Lyon, D. Richardson, H. Scantlebury (Eds.), Shreir's Corrosion, Elsevier, Oxford 2010, pp. 2205–2223.
[5] Cobalt, rhodium and iridium, in: N.N. Greenwood, A. Earnshaw (Eds.), Chemistry of the Elements, (second edition)Butterworth-Heinemann, Oxford 1997, pp. 1113–1143.
[6] J.A.V. Butler, G. Drever, The mechanism of electrolytic processes. Part I. The anodic oxidation of some metals of the platinum group, Trans. Faraday Soc. 32 (1936) 427–435.
[7] B.D. Kurnikov, A.I. Zhurin, V.V. Chernyi, Y.B. Vasil'ev, V.S. Bagotskii, Adsorption of oxygen on a smooth iridium electrode, Elektrokhimiya 9 (6) (1973) 833–836.
[8] J. Mozota, B.E. Conway, Surface and bulk processes at oxidized iridium electrodes—I. Monolayer stage and transition to reversible multilayer oxide film behaviour, Electrochim. Acta 28 (1) (1983) 1–8.
[9] J. Juodkazytė, B. Šebeka, G. Stalnionis, K. Juodkazis, EQCM study of iridium anodic oxidation in H2SO4 and KOH solutions, Electroanalysis 17 (19) (2005) 1734–1739.
[10] J. Juodkazytė, B. Šebeka, I. Valsiunas, K. Juodkazis, Iridium anodic oxidation to Ir(III) and Ir(IV) hydrous oxides, Electroanalysis 17 (11) (2005) 947–952.
[11] E.R. Kötz, H. Neff, Anodic iridium oxide films: a UPS study of emersed electrodes, Surf. Sci. 160 (2) (1985) 517–530.
[12] A.N. Chemodanov, I.M. July, Zashita metallov, Prot. Met. 27 (4) (1991) 658–666.
[13] P.G. Pickup, V.I. Birss, A model for anodic hydrous oxide growth at iridium, J. Electroanal. Chem. 220 (1) (1987) 83–100.
[14] B.E. Conway, J. Mozota, Surface and bulk processes at oxidized iridium electrodes—II. Conductivity-switched behaviour of thick oxide films, Electrochim. Acta 28 (1) (1983) 9–16.
[15] L.D. Burke, J.K. Mulcahy, D.P. Whelan, Preparation of an oxidized iridium electrode and the variation of its potential with pH, J. Electroanal. Chem. 163 (1–2) (1984) 117–128.
[16] L.D. Burke, D.P. Whelan, A voltammetric investigation of the charge storage reactions of hydrous iridium oxide layers, J. Electroanal. Chem. 162 (1–2) (1984) 121–141.
[17] J.M. Otten, W. Visscher, The anodic behaviour of iridium: I. The effect of potential cycling, J. Electroanal. Chem. 55 (1) (1974) 1–11.
[18] J.M. Otten, W. Visscher, The anodic behaviour of iridium: II. The oxygen coverage, J. Electroanal. Chem. 55 (1) (1974) 13–21.
[19] S. Gottesfeld, S. Srinivasan, Electrochemical and optical studies of thick oxide layers on iridium and their electrocatalytic activities for the oxygen evolution reaction, J. Electroanal. Chem. 86 (1) (1978) 89–104.
[20] D. Michell, D.A.J. Rand, R. Woods, Analysis of the anodic oxygen layer on iridium by X-ray emission, electron diffraction and electron microscopy, J. Electroanal. Chem. 84 (1) (1977) 117–126.
[21] R. Kötz, H. Neff, S. Stucki, Anodic iridium oxide films: XPS-studies of oxidation state changes and O_2 evolution, J. Electrochem. Soc. 131 (1) (1984) 72–77.
[22] R. Kötz, C. Barbero, O. Haas, Probe beam deflection investigation of the charge storage reaction in anodic iridium and tungsten oxide films, J. Electroanal. Chem. 296 (1) (1990) 37–49.
[23] V. Pfeifer, T.E. Jones, J.J. Velasco Vélez, C. Massué, R. Arrigo, D. Teschner, F. Girgsdies, M. Scherzer, M.T. Greiner, J. Allan, M. Hashagen, G. Weinberg, S. Piccinin, M. Hävecker, A. Knop-Gericke, R. Schlögl, The electronic structure of iridium and its oxides, Surf. Interface Anal. 48 (5) (2015) 261–273.
[24] V. Pfeifer, T.E. Jones, J.J. Velasco Velez, C. Massue, M.T. Greiner, R. Arrigo, D. Teschner, F. Girgsdies, M. Scherzer, J. Allan, M. Hashagen, G. Weinberg, S. Piccinin, M. Havecker, A. Knop-Gericke, R. Schlogl, The electronic structure of iridium oxide electrodes active in water splitting, Phys. Chem. Chem. Phys. 18 (4) (2016) 2292–2296.
[25] H.G. Sanchez Casalongue, M.L. Ng, S. Kaya, D. Friebel, H. Ogasawara, A. Nilsson, In situ observation of surface species on iridium oxide nanoparticles during the oxygen evolution reaction, Angew. Chem. Int. Ed. 53 (28) (2014) 7169–7172.
[26] A. Minguzzi, O. Lugaresi, E. Achilli, C. Locatelli, A. Vertova, P. Ghigna, S. Rondinini, Observing the oxidation state turnover in heterogeneous iridium-based water oxidation catalysts, Chem. Sci. 5 (9) (2014) 3591–3597.
[27] N. Danilovic, R. Subbaraman, K.-C. Chang, S.H. Chang, Y.J. Kang, J. Snyder, A.P. Paulikas, D. Strmcnik, Y.-T. Kim, D. Myers, V.R. Stamenkovic, N.M. Markovic, Activity–stability trends for the oxygen evolution reaction on monometallic oxides in acidic environments, J. Phys. Chem. Lett. 5 (14) (2014) 2474–2478.
[28] A.R. Hillman, M.A. Skopek, S.J. Gurman, X-ray spectroscopy of electrochemically deposited iridium oxide films: detection of multiple sites through structural disorder, Phys. Chem. Chem. Phys. 13 (12) (2011) 5252–5263.
[29] M. Hüppauff, B. Lengeler, Valency and structure of iridium in anodic iridium oxide films, J. Electrochem. Soc. 140 (3) (1993) 598–602.
[30] Y. Mo, I.C. Stefan, W.-B. Cai, J. Dong, P. Carey, D.A. Scherson, In situ iridium LIII-Edge X-ray absorption and surface enhanced Raman spectroscopy of electrodeposited iridium oxide films in aqueous electrolytes, J. Phys. Chem. B 106 (14) (2002) 3681–3686.
[31] T. Pauporté, D. Aberdam, J.-L. Hazemann, R. Faure, R. Durand, X-ray absorption in relation to valency of iridium in sputtered iridium oxide films, J. Electroanal. Chem. 465 (1) (1999) 88–95.
[32] D.N. Buckley, L.D. Burke, The oxygen electrode. Part 5.-enhancement of charge capacity of an iridium surface in the anodic region, J. Chem. Soc., Faraday Trans. 1 71 (0) (1975) 1447–1459.
[33] D.N. Buckley, L.D. Burke, The oxygen electrode. Part 6.-Oxygen evolution and corrosion at iridium anodes, J. Chem. Soc., Faraday Trans. 1 72 (1976) 2431–2440.
[34] S. Gottesfeld, J.D.E. McIntyre, Electrochromism in anodic iridium oxide films: II. pH effects on corrosion stability and the mechanism of coloration and bleaching, J. Electrochem. Soc. 126 (5) (1979) 742–750.
[35] M. Vuković, Voltammetric and galvanostatic studies of hydrous and anhydrous iridium oxide films, J. Appl. Electrochem. 20 (6) (1990) 969–973.
[36] M. Vuković, Oxygen evolution reaction on thermally treated iridium oxide films, J. Appl. Electrochem. 17 (4) (1987) 737–745.
[37] J.O. Zerbino, N.R. de Tacconi, A.J. Arvía, The activation and deactivation of iridium electrodes in acid electrolytes, J. Electrochem. Soc. 125 (8) (1978) 1266–1276.
[38] V. Birss, R. Myers, H. Angerstein-Kozlowska, B.E. Conway, Electron microscopy study of formation of thick oxide films on Ir and Ru electrodes, J. Electrochem. Soc. 131 (7) (1984) 1502–1510.
[39] P.G. Pickup, V.I. Birss, The influence of the aqueous growth medium on the growth rate, composition, and structure of hydrous iridium oxide films, J. Electrochem. Soc. 135 (1) (1988) 126–133.
[40] E.N. El Sawy, V.I. Birss, Nano-porous iridium and iridium oxide thin films formed by high efficiency electrodeposition, J. Mater. Chem. 19 (43) (2009) 8244–8252.
[41] T. Reier, M. Oezaslan, P. Strasser, Electrocatalytic Oxygen Evolution Reaction (OER) or Ru, Ir, and Pt Catalysts: A Comparative Study of Nanoparticles and Bulk Materials, ACS Catalysis 2 (8) (2012) 1765–1772.
[42] Y. Lee, J. Suntivich, K.J. May, E.E. Perry, Y. Shao-Horn, Synthesis and activities of rutile IrO 2 and RuO 2 nanoparticles for oxygen evolution in acid and alkaline solutions, J. Phys. Chem. Lett. 3 (3) (2012) 399–404.
[43] S. Siracusano, V. Baglio, A. Di Blasi, N. Briguglio, A. Stassi, R. Ornelas, E. Trifoni, V. Antonucci, A.S. Aricò, Electrochemical characterization of single cell and short stack PEM electrolyzers based on a nanosized IrO2 anode electrocatalyst, Int. J. Hydrog. Energy 35 (11) (2010) 5558–5568.
[44] I. Katsounaros, S. Cherevko, A.R. Zeradjanin, K.J.J. Mayrhofer, Nanostructured electrocatalysts – oxygen electrochemistry as a cornerstone for sustainable energy conversion, Angew. Chem. Int. Ed. 53 (2014) 102–121.
[45] M. Zeng, X.X. Wang, Z.H. Tan, X.X. Huang, J.N. Wang, Remarkable durability of Pt–Ir alloy catalysts supported on graphitic carbon nanocages, J. Power Sources 264(0) (2014) 272–281.
[46] K. Chakrapani, S. Sampath, The morphology dependent electrocatalytic activity of Ir nanostructures towards oxygen reduction, Phys. Chem. Chem. Phys. 16 (31) (2014) 16815–16823.
[47] M. Wesselmark, B. Wickman, C. Lagergren, G. Lindbergh, The impact of iridium on the stability of platinum on carbon thin-film model electrodes, Electrochim. Acta 111 (2013) 152–159.
[48] D.R. Merrill, M. Bikson, J.G.R. Jefferys, Electrical stimulation of excitable tissue: design of efficacious and safe protocols, J. Neurosci. Methods 141 (2) (2005) 171–198.
[49] H. Tsaprailis, V.I. Birss, Sol-gel derived Pt-Ir mixed catalysts for DMFC applications, Electrochem. Solid-State Lett. 7 (10) (2004) A348–A352.
[50] S.F. Cogan, Neural stimulation and recording electrodes, Annu. Rev. Biomed. Eng. 10 (1) (2008) 275–309.
[51] J. Qiao, R. Lin, B. Li, J. Ma, J. Liu, Kinetics and electrocatalytic activity of nanostructured Ir–V/C for oxygen reduction reaction, Electrochim. Acta 55 (28) (2010) 8490–8497.
[52] G. Topalov, G. Ganske, E. Lefterova, U. Schnakenberg, E. Slavcheva, Preparation and properties of thin Pt–Ir films deposited by dc magnetron co-sputtering, Int. J. Hydrog. Energy 36 (23) (2011) 15437–15445.
[53] D. Yang, B. Li, H. Zhang, J. Ma, Kinetics and electrocatalytic activity of IrCo/C catalysts for oxygen reduction reaction in PEMFC, Int. J. Hydrog. Energy 37 (3) (2012) 2447–2454.
[54] D.A.J. Rand, R. Woods, A study of the dissolution of platinum, palladium, rhodium and gold electrodes in 1 m sulphuric acid by cyclic voltammetry, J. Electroanal. Chem. 35 (1) (1972) 209–218.
[55] S. Cherevko, A.R. Zeradjanin, A.A. Topalov, N. Kulyk, I. Katsounaros, K.J.J. Mayrhofer, Dissolution of noble metals during oxygen evolution in acidic media, ChemCatChem 6 (8) (2014) 2219–2223.
[56] D.A.J. Rand, R. Woods, Cyclic voltammetric studies on iridium electrodes in sulphuric acid solutions: nature of oxygen layer and metal dissolution, J. Electroanal. Chem. 55 (3) (1974) 375–381.
[57] S. Cherevko, T. Reier, A.R. Zeradjanin, Z. Pawolek, P. Strasser, K.J.J. Mayrhofer, Stability of nanostructured iridium oxide electrocatalysts during oxygen evolution reaction in acidic environment, Electrochem. Commun. 48 (2014) 81–85.
[58] S. Cherevko, S. Geiger, O. Kasian, N. Kulyk, J.-P. Grote, A. Savan, B.R. Shrestha, S. Merzlikin, B. Breitbach, A. Ludwig, K.J.J. Mayrhofer, Oxygen and hydrogen evolution

reactions on Ru, RuO2, Ir, and IrO2 thin film electrodes in acidic and alkaline electrolytes: a comparative study on activity and stability, Catal. Today 262 (2016) 170–180.
[59] S.O. Klemm, A. Karschin, A.K. Schuppert, A.A. Topalov, A.M. Mingers, I. Katsounaros, K.J.J. Mayrhofer, Time and potential resolved dissolution analysis of rhodium using a microelectrochemical flow cell coupled to an ICP-MS, J. Electroanal. Chem. 677 (0) (2012) 50–55.
[60] A.A. Topalov, I. Katsounaros, J.C. Meier, S.O. Klemm, K.J.J. Mayrhofer, Development and integration of a LabVIEW-based modular architecture for automated execution of electrochemical catalyst testing, Rev. Sci. Instrum. 82 (2011) 114103.
[61] S. Cherevko, A.A. Topalov, A.R. Zeradjanin, I. Katsounaros, K.J.J. Mayrhofer, Gold dissolution: towards understanding of noble metal corrosion, RSC Adv. 3 (37) (2013) 16516–16527.
[62] A.A. Topalov, S. Cherevko, A.R. Zeradjanin, J.C. Meier, I. Katsounaros, K.J.J. Mayrhofer, Towards a comprehensive understanding of platinum dissolution in acidic media, Chem. Sci. 5 (2) (2014) 631–638.
[63] J.-P. Grote, A.R. Zeradjanin, S. Cherevko, K.J.J. Mayrhofer, Coupling of a scanning flow cell with online electrochemical mass spectrometry for screening of reaction selectivity, Rev. Sci. Instrum. 85 (10) (2014) 1041011–1041015.
[64] A.A. Topalov, I. Katsounaros, M. Auinger, S. Cherevko, J.C. Meier, S.O. Klemm, K.J.J. Mayrhofer, Dissolution of platinum: limits for the deployment of electrochemical energy conversion? Angew. Chem. Int. Ed. 51 (50) (2012) 12613–12615.
[65] S. Cherevko, A.A. Topalov, A.R. Zeradjanin, G.P. Keeley, K.J.J. Mayrhofer, Temperature-dependent dissolution of polycrystalline platinum in sulfuric acid electrolyte, Electrocatalysis 5 (3) (2014) 235–240.
[66] A.A. Topalov, A.R. Zeradjanin, S. Cherevko, K.J.J. Mayrhofer, The impact of dissolved reactive gases on platinum dissolution in acidic media, Electrochem. Commun. 40 (2014) 49–53.
[67] S. Cherevko, A.A. Topalov, I. Katsounaros, K.J.J. Mayrhofer, Electrochemical dissolution of gold in acidic medium, Electrochem. Commun. 28 (2013) 44–46.
[68] S. Cherevko, A.R. Zeradjanin, A.A. Topalov, G.P. Keeley, K.J.J. Mayrhofer, Effect of temperature on gold dissolution in acidic media, J. Electrochem. Soc. 161 (9) (2014) H501–H507.
[69] R. Woods, Hydrogen adsorption on platinum, iridium and rhodium electrodes at reduced temperatures and the determination of real surface area, J. Electroanal. Chem. 49 (2) (1974) 217–226.
[70] E.J. Frazer, R. Woods, The oxygen evolution reaction on cycled iridium electrodes, J. Electroanal. Chem. 102 (1) (1979) 127–130.
[71] S. Cherevko, A.R. Zeradjanin, G.P. Keeley, K.J.J. Mayrhofer, A comparative study on gold and Platinum dissolution in acidic and alkaline media, J. Electrochem. Soc. 161 (12) (2014) H822–H830.
[72] S. Cherevko, G.P. Keeley, S. Geiger, A.R. Zeradjanin, N. Hodnik, N. Kulyk, K.J.J. Mayrhofer, Dissolution of Platinum in the operational range of fuel cells, ChemElectroChem 2 (10) (2015) 1471–1478.
[73] M.L.B. Rao, A. Damjanovic, J.O.M. Bockris, Oxygen adsorption related to the unpaired d-electrons in transition metals, J. Phys. Chem. 67 (11) (1963) 2508–2509.
[74] A. Damjanovic, A. Dey, J.O.M. Bockris, Kinetics of oxygen evolution and dissolution on platinum electrodes, Electrochim. Acta 11 (7) (1966) 791–814.
[75] A. Damjanovic, M.K.Y. Wong, On the mechanism of oxygen evolution at iridium electrodes, J. Electrochem. Soc. 114 (6) (1967) 592–593.
[76] M.E.G. Lyons, S. Floquet, Mechanism of oxygen reactions at porous oxide electrodes. Part 2-oxygen evolution at RuO2, IrO2 and IrxRu1-xO2 electrodes in aqueous acid and alkaline solution, Phys. Chem. Chem. Phys. 13 (12) (2011) 5314–5335.
[77] K.J. Vetter, J.W. Schultze, The kinetics of the electrochemical formation and reduction of monomolecular oxide layers on platinum in 0.5 M H2SO4: Part I. Potentiostatic pulse measurements, J. Electroanal. Chem. 34 (1) (1972) 131–139.
[78] K.J. Vetter, J.W. Schultze, The kinetics of the electrochemical formation and reduction of monomolecular oxide layers on platinum in 0.5 M H2SO4: Part II. Galvanostatic pulse measurements and the model of oxide growth, J. Electroanal. Chem. 34 (1) (1972) 141–158.
[79] B.E. Conway, Electrochemical oxide film formation at noble-metals as a surface-chemical process, Prog. Surf. Sci. 49 (4) (1995) 331–452.
[80] F. Mao, S. Sharifi-Asl, J. Yu, D.D. Macdonald, Diagnosis of the mechanism of anodic oxide film growth on platinum in H2SO4, J. Electrochem. Soc. 161 (5) (2014) C254–C260.
[81] A. Sun, J. Franc, D.D. Macdonald, Growth and properties of oxide films on platinum: I. EIS and X-ray photoelectron spectroscopy studies, J. Electrochem. Soc. 153 (7) (2006) B260–B277.
[82] A. Sun, D.D. Macdonald, Growth and properties of oxide films on platinum II. pH dependence in alkaline solutions, ECS Trans. 2 (17) (2007) 1–10.
[83] H. Angerstein-Kozlowska, B.E. Conway, B. Barnett, J. Mozota, Role of ion adsorption in surface oxide formation and reduction at noble-metals - general features of the surface process, J. Electroanal. Chem. 100 (1–2) (1979) 417–446.
[84] B.E. Conway, B. Barnett, H. Angerstein-Kozlowska, B.V. Tilak, A surface-electrochemical basis for the direct logarithmic growth law for initial stages of extension of anodic oxide films formed at noble metals, J. Chem. Phys. 93 (11) (1990) 8361–8373.
[85] Y.M. Kolotyrkin, V.V. Losev, A.N. Chemodanov, Relationship between corrosion processes and oxygen evolution on anodes made from noble metals and related metal oxide anodes, Mater. Chem. Phys. 19 (1–2) (1988) 1–95.
[86] S. Cherevko, A.R. Zeradjanin, G.P. Keeley, K.J.J. Mayrhofer, A comparative study on gold and platinum dissolution in acidic and alkaline media, J. Electrochem. Soc. 161 (12) (2014) H822–H830.
[87] E.N. El Sawy, V.I. Birss, A comparative study of the electrodeposition of nanoporous Ir and Pt thin films, J. Electrochem. Soc. 160 (9) (2013) D386–D393.
[88] L.D. Burke, E.J.M. O'Sullivan, Oxygen gas evolution on hydrous oxides — an example of three-dimensional electrocatalysis? J. Electroanal. Chem. 117 (1) (1981) 155–160.
[89] M.M. Lohrengel, J.W. Schultze, Electrochemical properties of anodic gold oxide layers—I: potentiostatic oxide growth and double layer capacity, Electrochim. Acta 21 (11) (1976) 957–965.
[90] J.J. MacDonald, B.E. Conway, The role of surface films in the kinetics of oxygen evolution at Pd + Au alloy electrodes, Proceedings of the Royal Society of London, Series A. Math. Phys. Sci. 269 (1338) (1962) 419–440.
[91] S. Gottesfeld, Faradaic processes at the Ir/Ir oxide electrode, J. Electrochem. Soc. 127 (9) (1980) 1922–1925.
[92] P. Steegstra, M. Busch, I. Panas, E. Ahlberg, Revisiting the redox properties of hydrous iridium oxide films in the context of oxygen evolution, J. Phys. Chem. C 117 (40) (2013) 20975–20981.
[93] J. Augustynski, M. Koudelka, J. Sanchez, B.E. Conway, ESCA study of the state of iridium and oxygen in electrochemically and thermally formed iridium oxide films, J. Electroanal. Chem. 160 (1–2) (1984) 233–248.
[94] S. Fierro, T. Nagel, H. Baltruschat, C. Comninellis, Investigation of the oxygen evolution reaction on Ti/IrO2 electrodes using isotope labelling and on-line mass spectrometry, Electrochem. Commun. 9 (8) (2007) 1969–1974.
[95] D. Burke, M.E.G. Lyons, Electrochemistry of hydrous oxide films, in: J.O.M. Bockris, B.E. Conway, R.E. White (Eds.), Modern Aspects of Electrochemistry, 28, Plenum Press, 1996.